Theoretical Study of the Mechanism for the Oxidative Half-Reaction of Copper Amine Oxidase (CAO)

Rajeev Prabhakar* and Per E. M. Siegbahn

Department of Physics, Stockholm Centre for Physics, Astronomy and Biotechnology (SCFAB), Stockholm University, S-106 91 Stockholm, Sweden

Received: October 14, 2002; In Final Form: February 10, 2003

The oxidative half-reaction of copper amine oxidase (CAO) has been studied quantum mechanically using hybrid density functional theory (B3LYP). After the production of H_2O_2, two different but energetically similar mechanisms leading to the formation of ammonia and TPQ_{ox} are suggested. In one of the mechanisms (A), protonation of the O-2 site of the cofactor TPQ occurs prior to water activation whereas in the other (B) the O-2 site of the cofactor remains unprotonated. Both of these mechanisms are divided into four steps, and the last two steps in mechanism B are further divided into two steps. Detailed comparisons are made to experimental findings and suggestions. In particular, the roles of the copper metal center and the critical Asp319 are discussed.

I. Introduction

Copper amine oxidases (CAOs) constitute a class of enzymes that catalyze the oxidative deamination of primary amines to the corresponding aldehydes and ammonia, concomitant with the two-electron reduction of dioxygen to hydrogen peroxide. CAOs have diverse biological functions both in prokaryotes and in eukaryotes. In prokaryotes, they are suggested to be involved in nutrient metabolism,[1−3] and in eukaryotes, they are implicated in cell differentiation, cell growth, detoxification, wound healing, cell signaling, and programmed cell death.[4−8] In higher organisms, CAOs are suggested to be adhesion proteins that mediate the interaction between lymphocytes and endothelial cells and play an important role in inflammatory response.[9,10] Amine oxidases are homodimers with 70−95 kDa subunits with each subunit containing a cofactor, 2,4,5-trihydroxyphenylalanine-quinone, referred to as topa quinone (TPQ), and a copper ion.[8,11,12] The crystal structures from *Escherichia coli* (ECAO),[13] pea seedling (PSAO),[14] *Arthobactor globiformis* (APAO),[15] and yeast *Hansenula polymorpha* (HPAO)[16] have been solved. CAOs are proposed to be dual-function enzymes, catalyzing both cofactor biogenesis from an intrinsic, specific precursor tyrosine[17,18] and the oxidative deamination of amines.

The mechanism of copper-dependent amine oxidases has been reviewed recently.[19,20] Catalysis is suggested to proceed via a ping-pong mechanism[4,21] with two half-reactions known as the reductive and oxidative half-reactions, which are shown in eqs 1 and 2, respectively:

$$E_{ox} + RCH_2NH_2 \rightarrow E_{red} + RCHO \quad (1)$$

$$E_{red} + O_2 + H_2O \rightarrow E_{ox} + H_2O_2 + NH_3 \quad (2)$$

CAOs oxidize a range of primary amines with different amine oxidase enzymes having distinct substrate specificities. For example, PSAO prefers diamines as substrate and ECAO prefers aromatic amines whereas prokaryotic bacterial amine oxidase and mammalian plasma oxidases preferentially oxidize monoamines. Whether one or the other half-reaction is rate-limiting depends on the source of the enzyme.[22,23] The crystal structure of HPAO has been solved to 2.4-Å resolution.[16] In contrast to the earlier structures, this structure (see Figure 1) shows the cofactor already oriented as required for catalysis. At the active site, the C-5 carbonyl of the cofactor is directed toward the substrate binding site, and the active-site base (Asp319) is positioned at the right place for assisting in the Schiff base formation. The Cu atom is coordinated to the imidazole side-chains of three histidines, His456, His458, and His624, and to two water molecules, one equatorial and one axial in a distorted square-pyramidal geometry. The active-site base Tyr305 uses a hydrogen bonding network involving water molecules to connect the substrate binding site with the copper binding site.

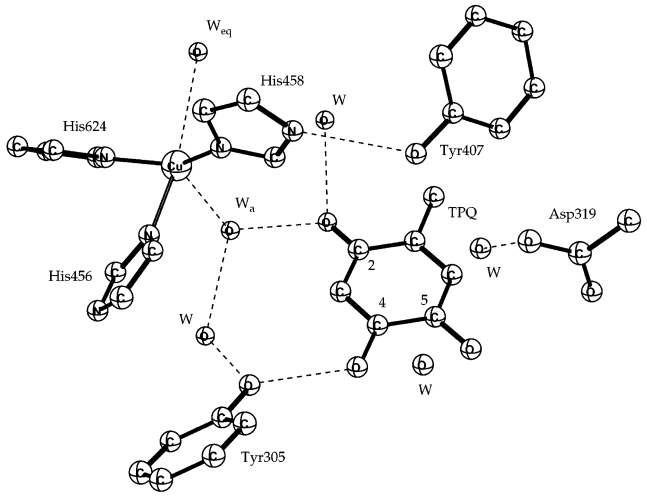

Figure 1. X-ray structure of the active-site region of HPAO.

In contrast to the detailed knowledge of the reductive half-reaction, much less is known about the mechanism for the oxidative half-reaction.[24−28] The oxidative half-reaction uses molecular oxygen to recycle the reduced enzyme back to its oxidized resting state accompanied by the release of ammonia and hydrogen peroxide. (See Figure 2.) In the first step of the suggested mechanism, O_2 enters the active site. The O_2 binding site was recently located for an X-ray structure of HPAO[16] as

* Corresponding author. E-mail: raju@physto.se.

10.1021/jp0272062 CCC: $25.00
Published on Web 04/02/2003

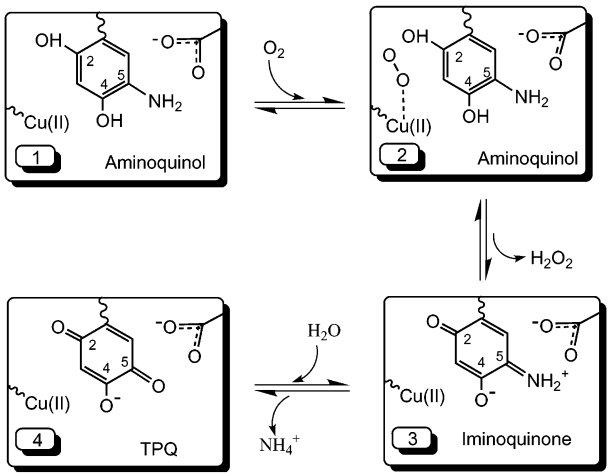

Figure 2. Experimentally suggested mechanism for the oxidative half-reaction of CAO.

the hydrophobic patch consisting of the amino acid side-chains from Leu, Met, and Tyr that lie very close to the O-2 position of the cofactor. This region is in the vicinity of the equatorial copper water and a crystal water molecule and is accessible to the hydrated dimer interface.[16] In the second step of the mechanism in Figure 2, dioxygen is reduced to hydrogen peroxide. There are two different versions of how this occurs.[26,28] In the "copper-on" mechanism, a superoxide ion is suggested to move and form a bond to copper whereas in the "copper-off" mechanism the superoxide ion does not bind to copper. In the first step of both versions, dioxygen is suggested to bind at a site near the O-2 position of TPQ. Dioxygen reduction is triggered by the first electron transfer from the reduced form of TPQ to the dioxygen, which leads to the formation of the superoxide ion. This first electron transfer is suggested to be the rate-limiting step. This step is followed by the successive transfers of the first proton, second electron, and second proton, which lead to the formation and release of H_2O_2. The O-4 proton is experimentally suggested to be involved in this process.[29] The second proton is most likely to be donated by the O-2 of TPQ. These proton transfers result in the formation of copper hydroxide and a protonated reduced cofactor. The reduction of dioxygen including the suggestion of a rate-limiting spin transition will be discussed in another paper[30] and will be only briefly discussed here.

In the remaining steps of the oxidative half-reaction, discussed in the rest of the paper, the reduced iminoquinone form of the cofactor is oxidized back to TPQ with the release of ammonia. The release of ammonia has been postulated to proceed either by the hydrolysis of the iminoquinone or by substrate transamination to form a substrate Schiff base.[19] The deprotonated Asp319 now accepts a proton from the water and triggers the nucleophilic attack by an activated water at the C-5 site of the cofactor, which results in a subsequent release of ammonia. The experimentally measured rate for the TPQ_{ox} oxidation of 7.4×10^{-2} s^{-1} corresponds to a barrier of 19.0 kcal/mol for the Cu-depleted enzyme, and 16.3 s^{-1} corresponds to a barrier of 15.8 kcal/mol in the presence of copper.[31] The crystal structure and a vast amount of available detailed experimental information provide an excellent starting point for the present quantum chemical study of the mechanism. Apart from testing the suggested mechanisms, quantum chemical studies can contribute by providing additional information about short-lived intermediates and transition states.

II. Computational Details

All calculations discussed in the present paper were performed using the Gaussian 98[32] and Jaguar[33] programs. The calculations for each structure were performed in two steps. First, an optimization of the geometry was made using the B3LYP method[34] with double-ζ-quality basis sets. For the second step of mechanism A, where the copper complex is included in the model, the LACVP basis set of Jaguar was used. This basis set has an effective core potential (ECP) for copper.[35] In the other steps of the mechanism, the d95 basis set was used for all atoms. Open-shell systems were treated using unrestricted B3LYP (UB3LYP). All degrees of freedom were optimized, and the transition states that were obtained were confirmed to have only one imaginary frequency of the Hessian. In the second step of the calculations, the B3LYP energy was evaluated for the optimized geometry using much larger basis sets. For the second step of mechanism A, the LACV3P** basis set of triple-ζ quality including one polarization function on each atom was used together with an ECP for the copper atom. In the other steps of the mechanism, the 6-311+G(2d,2p) basis set, which includes diffuse functions and two polarization functions on each atom, was used. Zero-point vibrational effects and thermal effects were added on the basis of B3LYP calculations using the same basis set as that used for the geometry optimization. The dielectric effects from the surrounding environment were obtained using the CPCM polarizable conductor model (Cosmo),[36] where the solvent cavity is formed as a surface of constant charge density of the solvated molecule. The default isodensity value of 0.0004 au was used. The radii of the solvent molecules were taken from the parameters for water. The united atom topological model[37] was used to build the cavity around each heavy atom, and the radius of each atomic sphere was determined by multiplying the van der Waals radius by a scaling factor of 1.2. For the second step of mechanism A, the self-consistent reaction-field method as implemented in Jaguar[38,39] was used to evaluate the solvent corrections by employing the LACVP basis set. A probe radius of $R = 1.40$ Å corresponding to the water molecule was chosen. In both cases, the dielectric constant was set equal to 4, which corresponds to a dielectric constant of about 3 for the protein and 80 for the water medium surrounding the protein.[40] Since models with the same charge were used throughout the present study, the relative dielectric effects were found to be rather small and not very sensitive to the method used or to the value chosen for the dielectric constant. The relative energies discussed below are Gibbs free energies where all of the effects described above are added. Normal errors of using B3LYP and different aspects of modeling enzyme active sites are described in recent reviews.[41−43]

III. Results and Discussion

The oxidative half-reaction of CAO has been studied using the B3LYP method and similar kinds of models as those used previously for the reductive half-reaction of PSAO.[44] The experimentally suggested mechanism shown in Figure 2 is used as a starting point for the present study. After the hydrogen peroxide-formation step, two different mechanisms were investigated. In HPAO, the active site is deeply buried and lies close to a interface between the two subunits of the enzyme.[16] Since CAOs are enzymes that utilize radical chemistry,[45] the active site is not directly accessible from bulk solvent. Substrate access requires a significant rearrangement of the polypeptide. The first question to be addressed here concerns the choice of an appropriate model for the active site. A neutral model for the active site was chosen, which should be reasonable for a

molecular system deeply buried in the low dielectric of a protein. Since the Cu metal center is experimentally suggested[19,26,28] to play a critical role in the first two steps of hydrogen peroxide formation and protonation of the O-2 site of TPQ, it is included in the model for these steps. The role of copper in the formation of hydrogen peroxide will be addressed in detail in a forthcoming paper.[30] In the other steps discussed here, the copper complex will be left out of the model. It is clear from experiments[46] that Asp319 is important in key steps of ammonia formation; therefore, it was also included in the model. After the formation of the product aldehyde in the reductive half-reaction, Asp319 is experimentally suggested to be unprotonated.[46] On the basis of these experimental suggestions, a negatively charged Asp319 is therefore included in the model. A neutral reduced aminoquinol form of TPQ, formed at the end of the reductive half-reaction in the previous B3LYP study,[44] is used in the first geometry optimization in mechanism A. It has also been suggested experimentally that after the formation of H_2O_2, TPQ is neutral.[28] This does not mean that the TPQ cofactor always remains neutral. As discussed below, in some of the steps, a negatively charged cofactor is found. In step 3 of mechanism B, two more water molecules were added to the model. One of the water molecules is observed in the crystal structure[16] whereas the second one is used to describe the hydrogen bonding from other active-site residues such as Tyr407. In step 3 of mechanism A, TPQ and Asp319 together carry a net neutral charge whereas in step 3 of mechanism B Asp319 carries a net negative charge. On the basis of earlier experience with the proton-transfer reactions, Asp319 is modeled by a formate. The detailed energetics for both mechanisms are summarized in Figures 22 and 23 and Tables 1 and 2.

A. Step 1. Mechanism for the Dioxygen Reduction. The mechanism for dioxygen reduction in the oxidative half-reaction will be presented in detail in a forthcoming paper.[30] Only the most important parts of the suggested mechanism will be briefly mentioned here. The reaction sequence of the dioxygen reduction to hydrogen peroxide can be written as

$$O_2 + TPQ_{aminoquinol} \rightarrow H_2O_2 + TPQ_{iminoquinone} \qquad (3)$$

The following mechanism is suggested by the B3LYP calculations. In the first step, as suggested experimentally, triplet dioxygen replaces the axial water (W_a) and binds between the O-2 and O-4 positions of the cofactor TPQ.[16,46] Dioxygen binding is accompanied by an electron transfer from the TPQ to dioxygen, which leads to the creation of a Cu(II)$\cdots O_2 \cdots$ M^+(rad) radical pair, where M^+(rad) represents the semiquinol form of TPQ. This radical pair is still in a triplet state. The electron-transfer step takes place without any enthalpy barrier, which does not necessarily mean that the formation of the radical pair is exergonic since there should be a large loss of entropy involved when the free O_2 becomes bound. In the next step, the superoxide anion crosses over a barrier of 8.2 kcal/mol and binds to copper. This step is endothermic by 2.6 kcal/mol. Once the Cu$-O_2^-$(rad) bonded species is formed, a proton transfer from O-2 and a hydrogen atom transfer from the O-4 site of the cofactor take place in a concerted manner. This concerted $2H^+ + e^-$ transfer leads to the formation of singlet H_2O_2 and the triplet form of the cofactor TPQ. Because of the formation of triplet TPQ, this step is quite endothermic—by 12.9 kcal/mol. After the formation of this species, a spin transition takes place because of the weak exchange between Cu and TPQ, and singlet TPQ is formed. This step is calculated to be exothermic by 29.1 kcal/mol. The T $\rightarrow$ S transition in cofactor TPQ is suggested to be the rate-limiting step for the entire oxidative half-reaction.

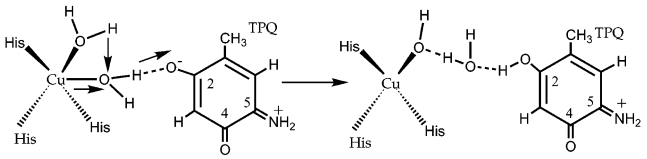

Figure 3. Suggested second step of mechanism A for the oxidative half-reaction.

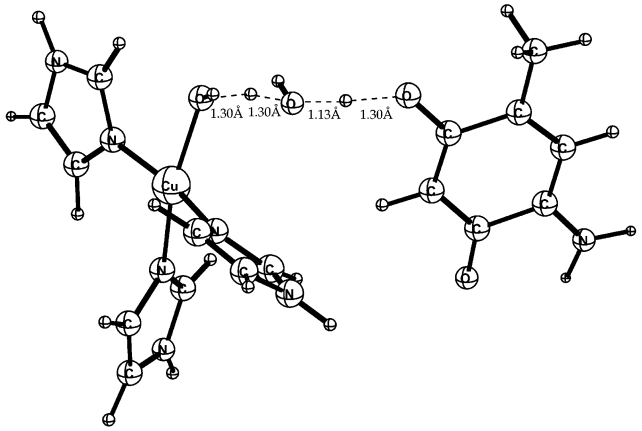

Figure 4. Optimized transition state for step 2 of mechanism A.

B. Step 2. Protonation of the O-2 Site of TPQ. After the formation of H_2O_2, the possibility of two different mechanisms arises. In mechanism A, the O-2 site of the cofactor is protonated whereas in mechanism B the O-2 site of the cofactor remains unprotonated. In the second step of mechanism A, shown in Figure 3, protonation of the O-2 site of cofactor TPQ takes place. Since the copper metal center is experimentally suggested to be involved in the protonation of the O-2 site,[19] the copper complex including three histidines and two water molecules (axial and equatorial) was included in the model. In this step, copper is initially pentacoordinated, and TPQ is hydrogen bonded to the axial water molecule. During the course of this step, the axial water becomes uncoordinated to copper and bridges between the equatorial water molecule and the O-2 site of cofactor TPQ. The formation of the intermediate structure in which copper is tetracoordinated is endergonic by 2.6 kcal/mol including zero-point vibrational (plus thermal enthalpy) effects of -1.4 kcal/mol, dielectric effects of $+3.8$ kcal/mol, and a calculated entropy effect of -0.5 kcal/mol. After the formation of this intermediate structure, a proton from the equatorial water is transferred to the O-2 position of the cofactor via the bridging water molecule. This proton transfer has a barrier of 2.8 kcal/mol including zero-point vibrational (plus thermal enthalpy) effects of -1.5 kcal/mol, dielectric effects of $+1.1$ kcal/mol, and a calculated entropy effect of -2.0 kcal/mol. Since the transition state follows a step that is endergonic by 2.6 kcal/mol, the overall barrier for the proton transfer is 5.4 kcal/mol. In the transition-state structure shown in Figure 4, a water molecule is located between the copper metal center and the O-2 position of the cofactor. This step is slightly endergonic by 1.8 kcal/mol including zero-point vibrational (plus thermal enthalpy) effects of -1.2 kcal/mol, dielectric effects of $+1.4$ kcal/mol, and a calculated entropy effect of $+2.5$ kcal/mol. The endergonicity of this step agrees well with the experimental suggestion that proton transfer from the Cu-coordinated water to TPQ should be energetically unfavorable because of the difference in pK_a values.[28] At the end of this step, protonated cofactor TPQ is formed.

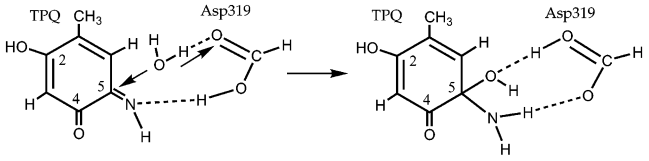

Figure 5. Suggested third step of mechanism A for the oxidative half-reaction.

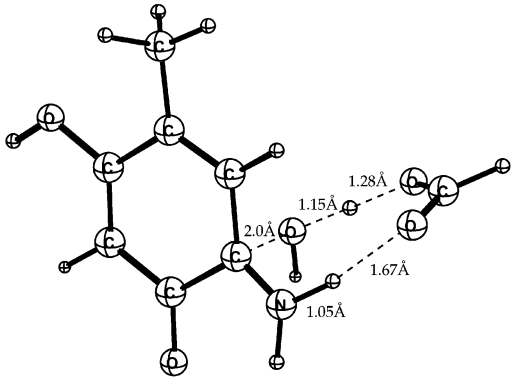

Figure 6. Optimized transition state for step 3 of mechanism A.

C. Step 3. Nucleophilic Attack by Water at the C-5 Site of TPQ. The suggested third step of mechanism A begins with a proton transfer from the NH_2^+ group at the C-5 site of cofactor TPQ to Asp319 (not included in the model of the first two steps). On the basis of an experimental suggestion,[46] an unprotonated Asp319 is chosen in this step. This proton transfer occurs spontaneously as the geometry of the reactant is optimized. The rest of the third step is shown in Figure 5 and describes the activation of a water molecule for a nucleophilic attack at the C-5 site of the TPQ cofactor. Apart from Asp319, the TPQ cofactor and a water molecule (to be activated) were included in the model, but not the copper complex. In this step, as suggested experimentally,[46] Asp319 plays one of its most important roles in the entire oxidative half-reaction. When the water molecule attacks C-5, a proton is donated to Asp319, and a C−O bond is formed. At the same time, Asp319 gives the previously abstracted proton back to the −NH group at the C-5 site of the cofactor.

This step has a barrier of 14.4 kcal/mol, which includes zero-point vibrational (plus thermal enthalpy) effects of −0.5 kcal/mol, dielectric effects of −1.1 kcal/mol, and a calculated entropy effect of +3.4 kcal/mol. The concerted transition state that is obtained is shown in Figure 6. This step is endergonic by 6.7 kcal/mol including zero-point vibrational (plus thermal enthalpy) effects of −1.7 kcal/mol and dielectric effects of +2.0 kcal/mol. At the end of this step, the C-5 site of the cofactor has both OH and NH_2 groups, and Asp319 is in a protonated form.

In mechanism B, the O-2 site is unprotonated prior to water activation. In the model for this mechanism, an unprotonated Asp319, the TPQ cofactor, a water molecule (to be activated), and two more additional solvent water molecules were included. In this step (see Figure 7), these two solvent water molecules are needed to provide stabilization of the active site through hydrogen bonding. One of the water molecules (W) is observed in the crystal structure[16] (see Figure 1), and the second water is used to take the hydrogen bonding contribution from active-site residue Tyr407 into account. Since in this mechanism TPQ is neutral and Asp319 is negative, the entire model that is used is negatively charged. Without the protonation of O-2, the water activation has a barrier of 17.1 kcal/mol, which includes zero-point vibrational (plus thermal enthalpy) effects of −1.8 kcal/mol and dielectric effects of −0.1 kcal/mol. The transition state that is obtained is shown in Figure 8. This step is quite endergonic by 14.4 kcal/mol including zero-point vibrational (plus thermal enthalpy) effects of −0.7 kcal/mol and dielectric effects of −0.3 kcal/mol. Since mechanism B has such a high barrier and is very endergonic, one more possibility was explored for the water activation in which a water molecule attacks the C-5 site of the protonated cofactor and transfers its proton to the NH_2 site of TPQ rather than to Asp319. However, the barrier for this process was found to be prohibitively high.

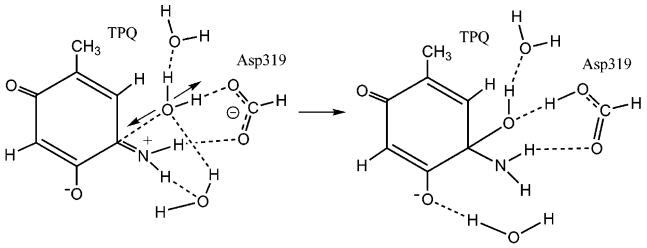

Figure 7. Suggested third step of mechanism B for the oxidative half-reaction.

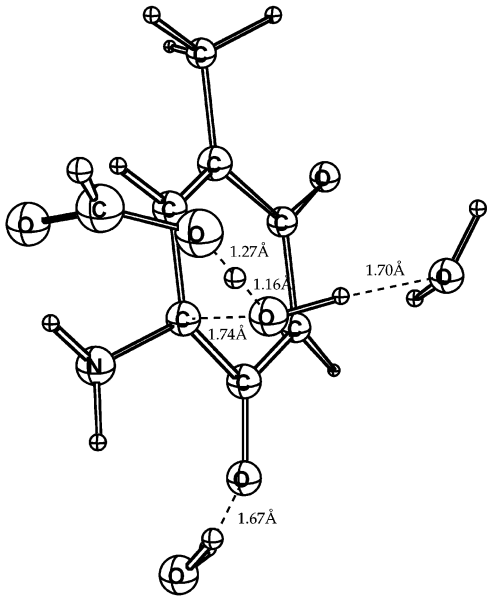

Figure 8. Optimized transition state for step 3 of mechanism B.

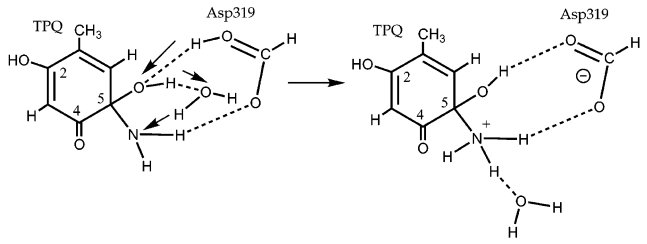

Figure 9. Suggested fourth step of mechanism A for the oxidative half-reaction.

D. Step 4. Formation of the NH_3 Group. In the proposed fourth step of mechanism A (see Figure 9), the hydroxyl proton from the C-5 position of TPQ is transferred to the NH_2 position of the cofactor. A water molecule is used to bridge the donor O-5 and acceptor NH_2 sites of TPQ. In a concerted manner, a proton from the O-5 hydroxyl group is transferred to the NH_2 position of the cofactor with a simultaneous transfer of the Asp319 proton to O-5 of TPQ. This proton transfer leads to the formation of an NH_3^+ group. Because of the positive charge on nitrogen, the NH_3 group formed in this step is not released

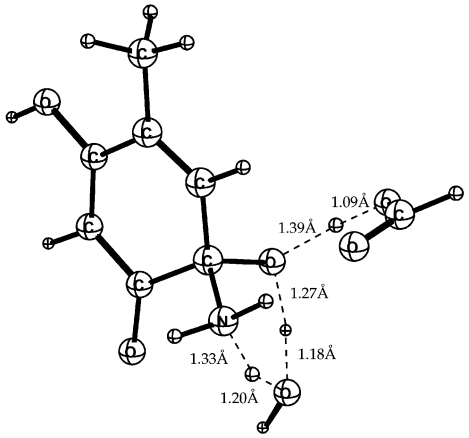

Figure 10. Optimized transition state for step 4 of mechanism A.

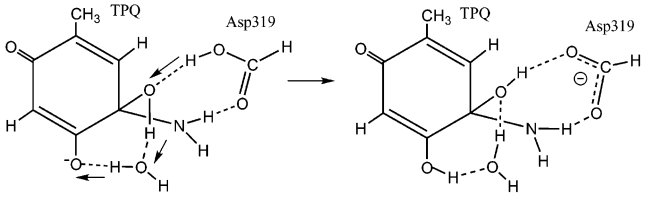

Figure 11. Suggested step 4a of mechanism B for the oxidative half-reaction.

to the protein but remains covalently bonded to the C-5 site of the cofactor. Strong hydrogen bonds stabilize this charge-separated system. This step has a barrier of 11.8 kcal/mol, which includes zero-point vibrational (plus thermal enthalpy) effects of −4.2 kcal/mol, dielectric effects of −0.9 kcal/mol, and an entropy effect of +2.0 kcal/mol. The optimized transition-state structure is shown in Figure 10. This step is exergonic by 4.9 kcal/mol including zero-point vibrational (plus thermal enthalpy) effects of −0.8 kcal/mol, dielectric effects of −3.6 kcal/mol, and an entropy effect of +0.5 kcal/mol. Since this step follows a step that is endergonic by 8.5 kcal/mol (see above), the overall barrier for this proton transfer becomes 20.3 kcal/mol.

In mechanism B, the fourth step is divided into two parts: 4a and 4b. In this step, a proton transfer from the C-5 hydroxyl to the NH_2 position of TPQ follows a two-step mechanism. Some attempts have been made to investigate a similar kind of one-step mechanism as suggested in mechanism A, but all of these attempts failed. It must be concluded that in the negatively charged state of the system it is energetically more favorable to have a two-step mechanism. When mechanism B is continued as shown in Figure 11, a proton from the hydroxyl group at the C-5 site is transferred to the O-4 site of the cofactor in step 4a. It has to be mentioned that during the optimization, proton itself moved to the O-4 site of TPQ. One solvent water molecule is used in the model to bridge the proton donor and acceptor sites of TPQ. This proton transfer occurs with the simultaneous donation of a proton by Asp319 to TPQ. This step has a barrier of 4.7 kcal/mol, which includes zero-point vibrational (plus thermal enthalpy) effects of −3.3 kcal/mol, dielectric effects of +2.1 kcal/mol, and a calculated entropy effect of +1.0 kcal/mol. The optimized transition state for this step is shown in Figure 12. Since this step follows a step that is endergonic by 14.4 kcal/mol, the overall barrier for this proton transfer becomes 19.1 kcal/mol. This step is exergonic by 4.0 kcal/mol including zero-point vibrational (plus thermal enthalpy) effects of +1.4 kcal/mol, dielectric effects of +1.1 kcal/mol, and an entropy effect of +0.5 kcal/mol. At the end of this step, cofactor TPQ is neutral, and Asp319 carries the negative charge of the system.

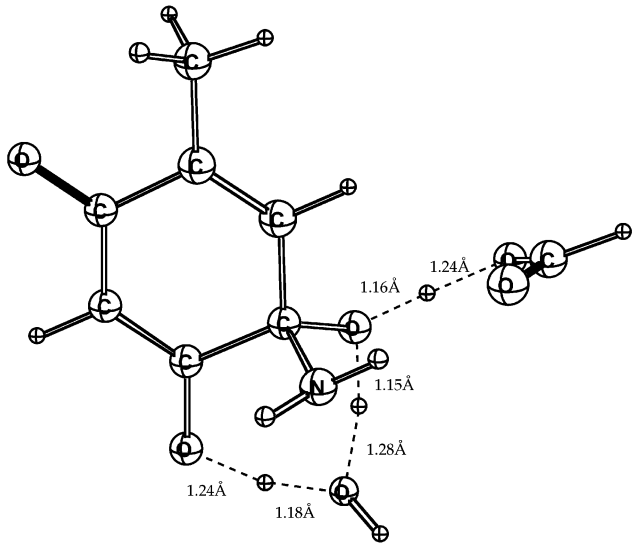

Figure 12. Optimized transition state for step 4a of mechanism B.

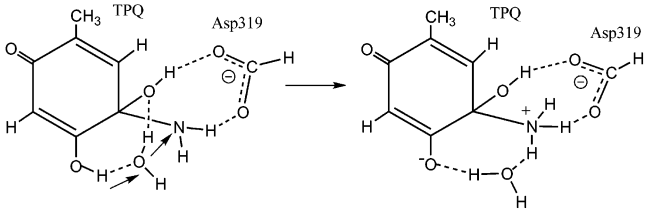

Figure 13. Suggested step 4b of mechanism B for the oxidative half-reaction.

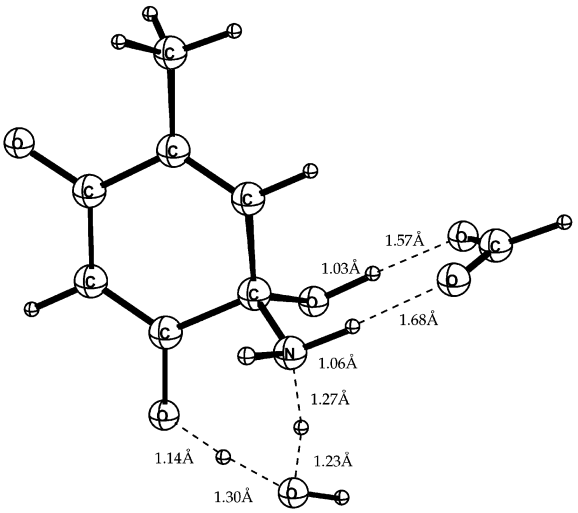

Figure 14. Optimized transition state for step 4b of mechanism B.

In step 4b, the proton that was transferred to the O-4 site is transferred again, as shown in Figure 13, but this time to the NH_2 position of the cofactor. The same bridging water molecule as that used earlier is used to bridge the donor O-4 and acceptor NH_2 sites of TPQ. The optimized transition state for this step is shown in Figure 14. The proton transfer in step 4 leads to the formation of an NH_3^+ group. Again, because of the positive charge on nitrogen, the NH_3 group formed in this step is not released to the protein but remains covalently bonded to the C-5 site of the cofactor. This charge-separated system is again stabilized by strong hydrogen bonds. This step has a very small barrier of 2.1 kcal/mol and is exergonic by 7.6 kcal/mol. Solvent effects favor the product by 6.90 kcal/mol, which is mainly due to a rather large change in the dipole moment from 3.4 D for

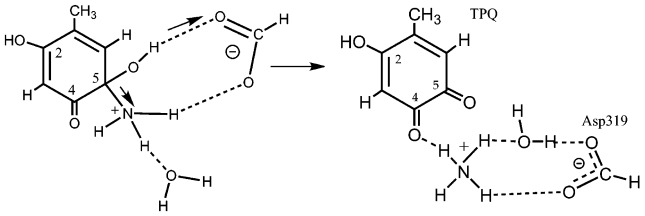

Figure 15. Suggested step 5 of mechanism A for the oxidative half-reaction.

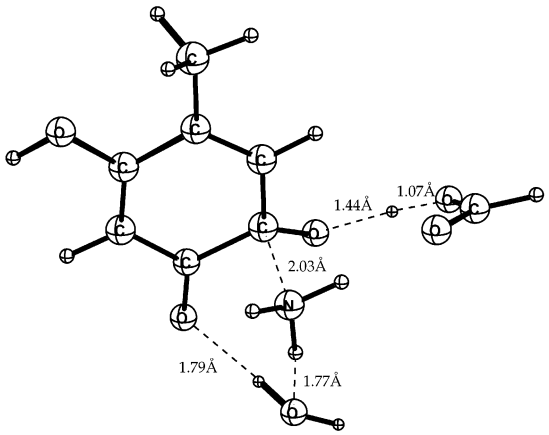

Figure 16. Optimized transition state for step 5 in mechanism A.

the reactant to 5.9 D for the product. Thus, from the production of H_2O_2 to the formation of the NH_3 group, the overall barrier of 19.1 kcal/mol for mechanism B is slightly lower than the barrier of 20.3 kcal/mol for mechanism A. However, it is clear that the accuracy of the present methods is not sufficient to discriminate between these two energetically very similar pathways.

E. Step 5. Release of Ammonia as an Ammonium Ion. In the suggested fifth step of mechanism A (see Figure 15), a rather large structural rearrangement takes place. In a somewhat complicated process, the hydroxyl proton at the C-5 position is transferred to the Asp319, which swings around and donates this proton to the NH_3^+ group. In this process, the ammonium ion is released from its position at the cofactor and moves all the way to form a hydrogen bond at the O-4 site of the TPQ cofactor. All of these changes occurred automatically during the stepwise optimization. This step has a barrier of 6.0 kcal/mol, which includes zero-point vibrational (plus thermal enthalpy) effects of −0.7 kcal/mol, dielectric effects of +2.3 kcal/mol, and an entropy effect of −1.2 kcal/mol. The optimized transition-state structure is shown in Figure 16. This step is exergonic by 7.5 kcal/mol including zero-point vibrational (plus thermal enthalpy) effects of +0.2 kcal/mol and dielectric effects of −0.4 kcal/mol. The entropy effect of −4.8 kcal/mol (included in the values) favors the product and is due to the release of the ammonium ion. At the end of this step, a neutral TPQ, a negatively charged Asp319, and an ammonia molecule are formed, in full agreement with experiments.[19,31,46]

In mechanism B, the step leading to the formation of the ammonium ion is again divided into two steps: 5a and 5b. In step 5a, as shown in Figure 17, some reorganization of the hydrogen bonds take place. In this step, a hydrogen bond between the O-5 hydroxyl group at the C-5 site and Asp319 is broken, and a new hydrogen bond between this hydroxyl group and the bridging water molecule is formed. Another noticeable change in this step is that one of the protons from the NH_3^+ group moves toward Asp319 and sits between the nitrogen and

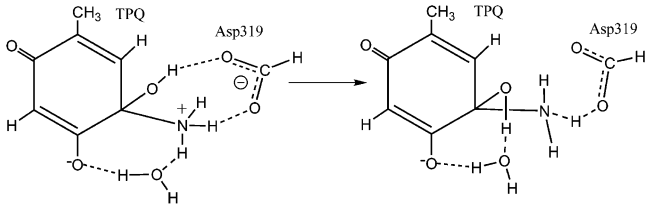

Figure 17. Suggested step 5a of mechanism B for the oxidative half-reaction.

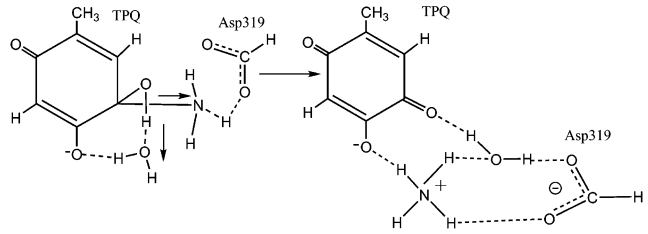

Figure 18. Suggested step 5b of mechanism B for the oxidative half-reaction.

oxygen atoms of NH_2 and Asp319, respectively. In the structure, the $N-H^+$ bond length is 1.21 Å, and the $O-H^+$ bond length is 1.30 Å. This is a true minimum since the Hessian has no imaginary frequency. This step is endergonic by 9.4 kcal/mol, where zero-point vibrational (plus thermal enthalpy) effects contribute −2.0 kcal/mol and dielectric effects, +4.0 kcal/mol. The calculated entropy effect is −1.0 kcal/mol (included in the values), favoring the product. Since the barrier from the product side is very small, the transition-state optimization failed for this step. This problem was set aside since the size of a very small barrier does not have any impact on the mechanism. In the next step (5b), as shown in Figure 18, a hydroxyl proton at the C-5 position is transferred to the bridging water molecule in a similar manner to that discussed for mechanism A. At the same time, Asp319 swings around and abstracts this proton from the water and donates it to the NH_3^+ group. During this process, the ammonium ion is released from its position at the cofactor and moves to form a hydrogen bond at the O-4 site of the TPQ cofactor. Again, all of these changes occurred automatically during the stepwise optimization.

This step has a barrier of 6.4 kcal/mol, which includes zero-point vibrational (plus thermal enthalpy) effects of −0.6 kcal/mol, dielectric effects of +0.4 kcal/mol, and an entropy effect of +1.3 kcal/mol. The optimized transition-state structure is shown in Figure 19. This step is exergonic by 18.8 kcal/mol including zero-point vibrational (plus thermal enthalpy) effects of +2.2 kcal/mol and dielectric effects of +1.3 kcal/mol. The entropy effect of −2.3 kcal/mol (included in the values) favors the product and is due to the release of the ammonium ion. In mechanism A, at the end of the oxidative half-reaction, a proton at O-2 is transferred back to the copper complex, and the enzyme is prepared for the next catalytic cycle. This step is beyond the scope of this study; therefore, it is not investigated here. However, a possible proton transfer from the ammonium ion to the O-4 site of the cofactor was also investigated. A few attempts were made in this direction, but they all led to very endergonic reactions. It is therefore suggested that TPQ obtains a proton from the surrounding enzyme. An example of this kind of mechanism was suggested for PSAO, where at the beginning of the reductive half-reaction Lys296 protonates the O-4 site of TPQ.[44] In other CAOs, for example, in BSAO, TPQ could be negatively charged at the beginning of the reductive half-reaction.

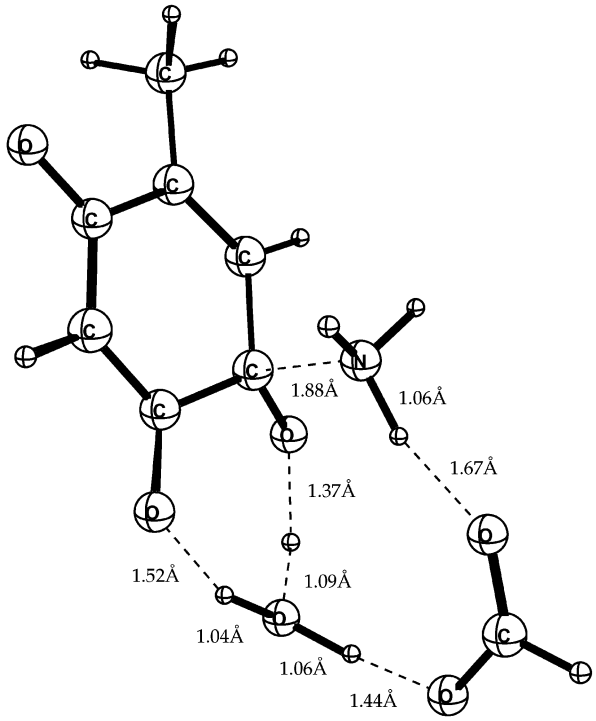

Figure 19. Optimized transition state for step 5b of mechanism B.

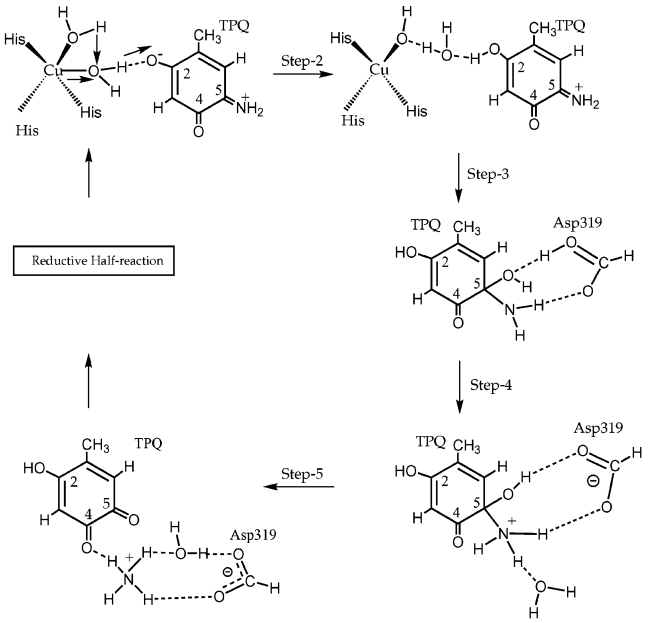

Figure 20. Theoretically suggested mechanism A for the oxidative half-reaction of CAO.

IV. Summary

The oxidative half-reaction of CAO has been studied using similar kinds of computational methods and models to those used previously for the reductive half-reaction of PSAO[44] and for different substrate reactions of other enzymes such as RNR[47,48] and PFL.[49] The present quantum chemical study was strongly directed by the structural and spectroscopic information provided by experiments. Two different but energetically similar mechanisms, A and B, were studied. The first step is common to both mechanisms, and it is only after the formation of H_2O_2 that the two mechanisms start to deviate. The different steps of mechanisms A and B are described in Figures 20 and 21. The detailed energetics is shown in Figures 22 and 23 and Tables 1 and 2. It is shown that after the H_2O_2-formation step the energy

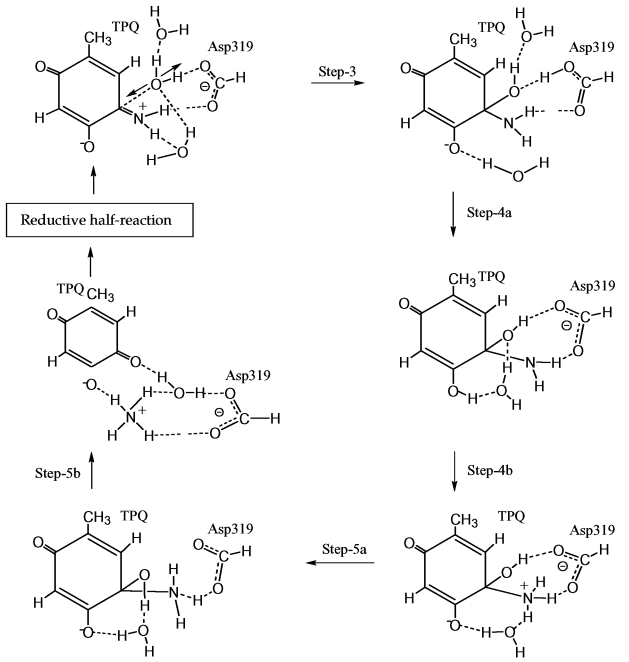

Figure 21. Theoretically suggested mechanism B for the oxidative half-reaction of CAO.

diagrams for both mechanisms are divided into four steps. The energy diagrams are constructed by imposing the condition that the reactant of each step has the same energy as the product of the previous step. At the starting point of the presently suggested mechanism, dioxygen occupies a cavity between the O-2 and O-4 positions of the cofactor. Endergonic binding of dioxygen is followed by an electron transfer leading to the creation of a triplet Cu(II)$\cdots O_2^-$(rad)$\cdots M^+$(rad) system. In the next step, O_2^- crosses over a barrier of 8.2 kcal/mol and binds to copper. Once the Cu$-O_2^-$ bonded species is formed, a proton transfer from O-2 and a hydrogen atom transfer from the O-4 site of the cofactor take place in a concerted manner. This concerted $2H^+ + e^-$ transfer leads to the formation of singlet H_2O_2 and a triplet form of cofactor TPQ. Because of the weak exchange interaction in the Cu(doublet)$\cdots$TPQ(triplet) system, a spin flipping takes place, and singlet TPQ is formed. The T $\rightarrow$ S transition is proposed to be the rate-limiting step for the entire oxidative half-reaction.

In mechanism A, the TPQ cofactor is protonated at the O-2 position by the copper complex prior to water activation. In the third step, water activation takes place with a barrier of 14.4 kcal/mol. In the fourth step, a proton transfer from the O-5 hydroxyl group to the NH_2 group at the O-5 position of the TPQ forms a bonded NH_3 group. This step has a barrier of 11.8 kcal/mol, but since this step follows an endergonic step, the overall barrier for this step becomes 20.3 kcal/mol. In the last step, a proton abstraction by Asp319 triggers the release of an ammonium ion with the simultaneous formation of a neutral topaquinone and an unprotonated Asp319. This step has a barrier of 6.0 kcal/mol. The present mechanism, as described in Figure 22, is in line with most of the available experimental information. As shown in Figure 23, the energy diagram for mechanism B is also divided into four steps, where the third and fourth steps are further divided into two steps. In mechanism B, the TPQ cofactor remains unprotonated at O-2 in the water activation step, which passes over a barrier of 17.1 kcal/mol. In the third step, a proton is transferred from the C-5 to the O-4 site of TPQ with a barrier of 4.7 kcal/mol. Since this step follows an endergonic step, the overall barrier for this step

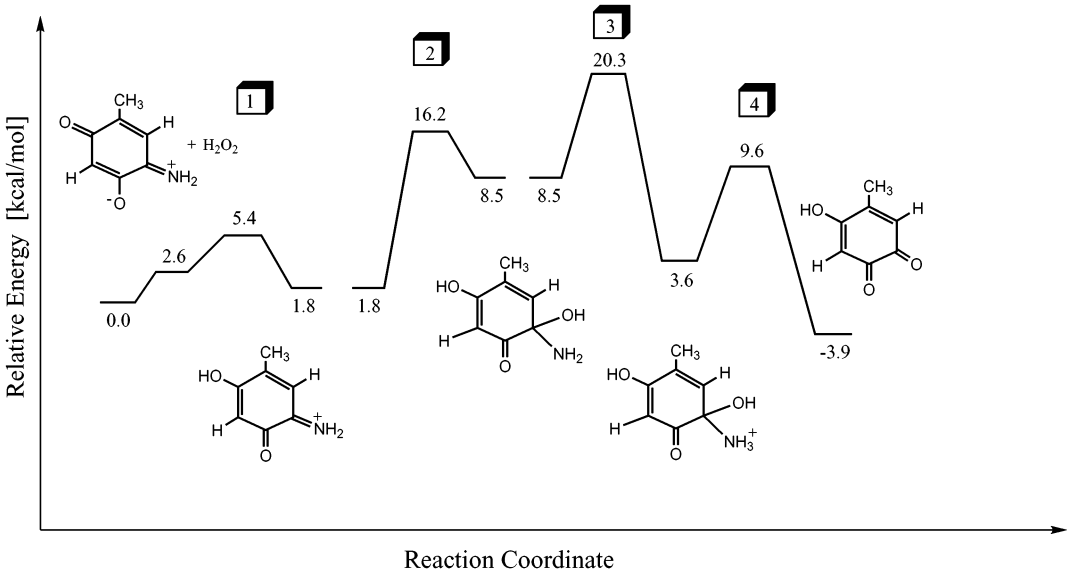

Figure 22. Energy diagram for mechanism A for the oxidative half-reaction.

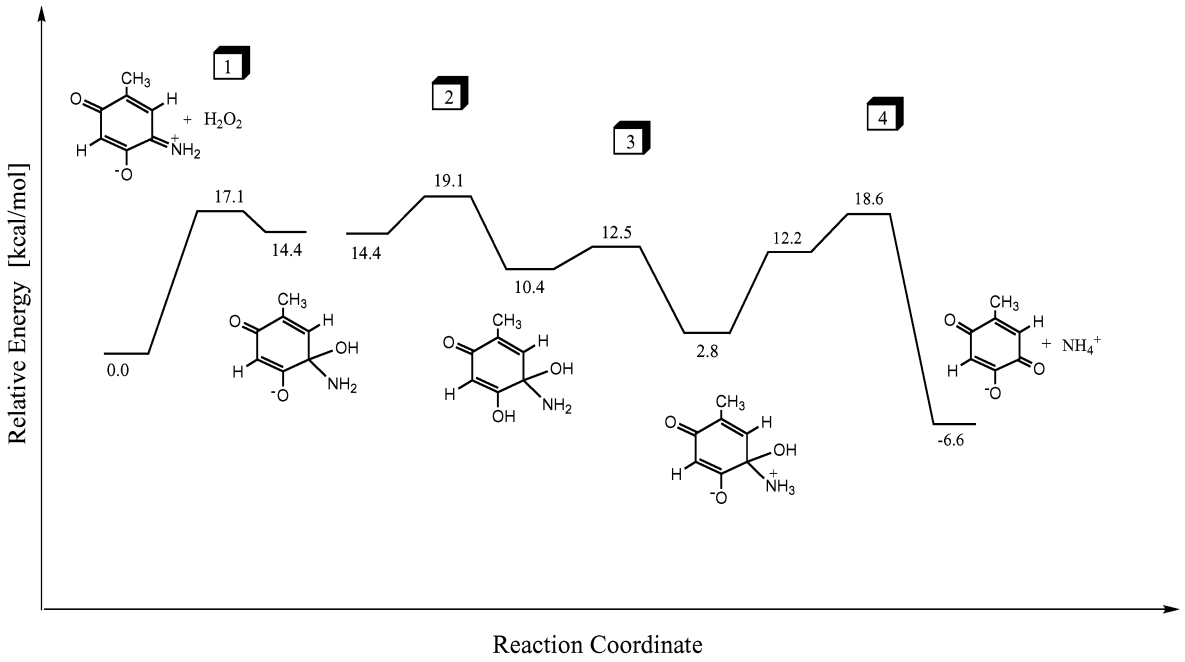

Figure 23. Energy diagram for mechanism B for the oxidative half reaction.

becomes 19.1 kcal/mol. In the fourth step, a proton transfer from the O-4 to the NH_2 group at the O-5 position of TPQ leads to a bonded NH_3^+ group. In step 5, a rearrangement of the hydrogen bonds takes place, but the key change is the formation of a hydrogen bond between the C-5 hydroxyl group and a bridging water molecule. This bond is important for the release of ammonia. In the last step, the transfer of the O-5 hydroxyl proton to the neighboring water molecule triggers the release of the ammonium ion with the simultaneous formation of a negatively charged topaquinone and an unprotonated Asp319.

The formation of these species has been suggested experimentally.[31,46] This step has a barrier of 6.4 kcal/mol and is exergonic by 18.8 kcal/mol. The present mechanisms as described in Figures 20 and 21 are energetically very similar and in line with most of the available experimental information. Although they are energetically very similar, there are significant differences in these two mechanisms. For example, in step 3 of mechanism A, the system is neutrally charged whereas in mechanism B the whole system starts out negatively charged. In this step, two additional water molecules were required to obtain the same reaction. Another notable difference is in step 4, where in mechanism A only one step is needed to transfer a proton from the O-5 hydroxyl group to the NH_2 group at the O-5 position of TPQ but in mechanism B two steps are required to achieve the same proton transfer. It is therefore clear that the overall charge state of the model plays a crucial role in determining the reaction pathways. The accuracy of the available methods is not sufficient to determine which one of the underlying mechanisms is most probable. The main question to be considered here is if, prior to the water activation step, a protonation of the O-2 site of the cofactor takes place. Here it has to be stressed that since the T → S nonradiative transition is suggested to be rate-limiting for the entire oxidative half-reaction,[30] which one of the above-mentioned mechanisms the enzyme utilizes would not affect the overall rate of the reaction. The highest barriers in the oxidative half-reaction computed in

TABLE 1: Energies (kcal/mol) of the Optimized Structures for the Different Steps of Mechanism A

	E_{bigbasis}	E_{DZ}	$E_{\Delta H}$[a]	E_{solv}[b]	$E_{T\Delta S}$
step 2					
0.0	0.0	0.0	0.0	0.0	0.0
2.6	0.6	−2.2	−1.3	3.8	−0.5
5.4	5.7	−1.4	−2.9	4.9	−2.4
1.8	−3.0	−6.5	−2.5	5.2	2.0
step 3					
1.8	0.0	0.0	0.0	0.0	0.0
16.2	12.5	3.8	−0.5	−1.1	3.4
8.5	4.6	−0.7	−1.7	2.0	1.7
step 4					
8.5	0.0	0.0	0.0	0.0	0.0
20.3	14.9	5.6	−4.2	−0.9	2.0
3.6	−1.1	−3.4	−0.8	−3.6	0.5
step 5					
3.6	0.0	0.0	0.0	0.0	0.0
9.6	5.6	8.5	−0.7	2.3	−1.2
−3.9	−2.4	−4.3	0.2	−0.4	−4.8

[a] Sum of zero-point and thermal enthalpy effects. [b] Calculated with the DZ basis set.

TABLE 2: Energies (au) of the Optimized Structures for the Different Steps of Mechanism B

	E_{bigbasis}	E_{DZ}	$E_{\Delta H}$[a]	E_{solv}[b]	$E_{T\Delta S}$
step 3					
0.0	0.0	0.0	0.0	0.0	0.0
17.1	17.2	15.9	−1.8	−0.1	1.8
14.4	14.6	15.6	−0.7	−0.3	0.8
step 4a					
14.4	0.0	0.0	0.0	0.0	0.0
19.1	4.90	0.9	−3.3	2.1	1.0
10.4	−7.0	−3.7	1.4	1.1	0.5
step 4b					
10.4	0.0	0.0	0.0	0.0	0.0
12.5	5.3	−0.7	−3.2	−1.5	1.5
2.8	−1.6	−4.5	0.4	−6.9	0.5
step 5a					
2.8	0.0	0.0	0.0	0.0	0.0
12.2	8.3	−8.3	−2.0	4.0	−1.0
step 5b					
12.2	0.0	0.0	0.0	0.0	0.0
18.6	5.3	0.19	−0.6	0.4	1.3
−6.6	−19.9	−21.0	2.2	1.3	−2.3

[a] Sum of zero-point and thermal enthalpy effects. [b] Calculated with the DZ basis set.

the present study of 18−20 kcal/mol are somewhat higher than the experimentally measured value of 15.8 kcal/mol, but taking the accuracy of the present methods into account, the agreement must still be considered to be quite satisfactory. In addition to the known information, the model calculations have suggested two different mechanisms and provided new insight into the catalytic function of this enzyme.

References and Notes

(1) Parrott, S.; Jones, S.; Cooper, R. A. *J. Gen. Microbiol.* **1987**, *133*, 347−351.

(2) Cooper, R. A.; Knowles, P. F.; Brown, D. E.; McGuirl, M. A.; Dooley, D. M. *Biochem. J.* **1992**, *288*, 337−340.

(3) Hacisalihoglu, A.; Jongejan, J. A.; Duine, J. A. *Microbiology* **1997**, *143*, 505−512.

(4) McIntire, W. S.; Hartmann, C. Copper Containing Amine Oxidases. In *Principles and Application of Quinoproteins*; Davidson, V. L., Ed.; Marcel Dekker: New York, 1993; pp 97−171.

(5) Klinman, J. P.; Mu, D. *Annu. Rev. Biochem.* **1994**, *63*, 299−344.

(6) McIntire, W. S. *Annu. Rev. Nutr.* **1998**, *18*, 145−177.

(7) Möller, S. G.; McPherson, M. J. *Plant J.* **1998**, *13*, 781−791.

(8) Knowles, P. F.; Dooley, D. M. In *Metal Ions in Biological Systems*; Sigel, H., Sigel A., Eds.; Marcel Dekker: New York, 1994; Vol. 30, p 361.

(9) Bono, P.; Salmi, M.; Smith, D. J.; Jalkanen, S. *J. Immunol.* **1998**, *160*, 5563−5571.

(10) Smith, D. J.; Salmi, M.; Bono, P.; Hellman, J.; Leu, T.; Jalkanen, S. *J. Exp. Med.* **1998**, *188*, 17−27.

(11) McIntire, W. S. *FASEB J.* **1994**, *8*, 513.

(12) Tanizawa, K. J. *Biochemistry* **1995**, *118*, 671.

(13) Parsons, M. R.; Convery, M. A.; Wilmot, C. M.; Yadav, K. D. S.; Blakeley, V.; Corner, A. S.; Phillips, S. E. V.; McPherson, M. J.; Knowles, P. F. *Structure* **1995**, *3*, 1171−1184.

(14) Kumar, V.; Dooley, D. M.; Freeman C. H.; Guss, J. M.; Harvy, I.; McGuirl, M. A.; Wilce, M. C. J.; Zubak, V. M. *Structure* **1996**, *4*, 943−955.

(15) Wilce, M. C. J.; Dooley, D. M.; Freeman C. H.; Guss, J. M.; Matsunami, H.; McIntire, W. S.; Ruggiero, C. E.; Tanizawa, K.; Yamaguchi, H. *Biochemistry* **1997**, *36*, 16116−16133.

(16) Li, R.; Klinman, J. P.; Mathews, F. S. *Structure* **1998**, *6*, 293−307.

(17) Cai, D.; Klinman, J. P. *J. Biol. Chem.* **1994**, *269*, 32039−32042.

(18) Matsuzaki, R.; Fukui, T.; Sato, H.; Ozaki, Y.; Tanizawa, K. *FEBS Lett.* **1994**, *351*, 360−364.

(19) Klinman, J. P. *Chem. Rev.* **1996**, *96*, 2541−2561.

(20) Stubbe, J.; Van der donk, W. A. *Chem. Rev.* **1998**, *98*, 705−762.

(21) Knowles, P. F.; Yadav, D. S. In *Copper Proteins and Copper Enzymes*; Lontie, R., Ed.; CRC Press: Boca Raton, FL, 1984; p 103.

(22) Lindström, A.; Petterson, G. *Eur. J. Biochem.* **1978**, *84*, 479−485.

(23) Rius, F. X.; Knowles, P. F.; Petterson, G. *Biochem. J.* **1984**, *220*, 767−772.

(24) Dooley, D. M.; Cote, C. E.; Golnik, K. C. *J. Mol. Catal.* **1984**, *23*, 243−253.

(25) Suzuki, S.; Sakurai, T.; Nakahara, A.; Manabe, T.; Okuyama, T. *Biochemistry* **1983**, *22*, 1630−1635.

(26) Dooley, D. M.; McGuirl, M. A.; Brown, D. E.; Turowski, P. N.; McIntire, W. S.; Knowles, P. F. *Nature (London)* **1991**, *349*, 262−264.

(27) Turowski, P. N.; McGuirl, M. A.; Dooley, D. M. *J. Biol. Chem.* **1993**, *268*, 17680−17682.

(28) Qiaojuan, S.; Klinman, J. P. *Biochemistry* **1998**, *37*, 12513−12525.

(29) Farnum, M.; Palcic, M. M.; Klinman, J. P. *Biochemistry* **1986**, *25*, 1898−1904.

(30) Prabhakar, R.; Siegbahn, P. E. M.; Minaev, B. F.; Ågren, H. To be submitted for publication.

(31) Mills, S. A.; Klinman, J. P. *J. Am. Chem. Soc.* **2000**, *122*, 9897−9904.

(32) Frisch, M. J.; Trucks, G. W.; Schlegel, H. B.; Scuseria, G. E.; Robb, M. A.; Cheeseman, J. R.; Zakrzewski, V. G.; Montgomery, J. A., Jr.; Stratmann, R. E.; Burant, J. C.; Dapprich, S.; Millam, J. M.; Daniels, A. D.; Kudin, K. N.; Strain, M. C.; Farkas, O.; Tomasi, J.; Barone, V.; Cossi, M.; Cammi, R.; Mennucci, B.; Pomelli, C.; Adamo, C.; Clifford, S.; Ochterski, J.; Petersson, G. A.; Ayala, P. Y.; Cui, Q.; Morokuma, K.; Malick, D. K.; Rabuck, A. D.; Raghavachari, K.; Foresman, J. B.; Cioslowski, J.; Ortiz, J. V.; Stefanov, B. B.; Liu, G.; Liashenko, A.; Piskorz, P.; Komaromi, I.; Gomperts, R.; Martin, R. L.; Fox, D. J.; Keith, T.; Al-Laham, M. A.; Peng, C. Y.; Nanayakkara, A.; Gonzalez, C.; Challacombe, M.; Gill, P. M. W.; Johnson, B. G.; Chen, W.; Wong, M. W.; Andres, J. L.; Head-Gordon, M.; Replogle, E. S.; Pople, J. A. *Gaussian 98*; Gaussian, Inc.: Pittsburgh, PA, 1998.

(33) *JAGUAR 4.1*; Schrödinger, Inc.: Portland, OR, 2000. See Vacek, G.; Perry, J. K.; Langlois, J.-M. *Chem. Phys. Lett.* **1999**, *310*, 189−194.

(34) Becke, A. D. *Phys. Rev. A* **1988**, *38*, 3098. Becke, A. D. *J. Chem. Phys.* **1993**, *98*, 1372. Becke, A. D. *J. Chem. Phys.* **1993**, *98*, 5648.

(35) Hay, P. J.; Wadt, W. R. *J. Chem. Phys.* **1985**, *82*, 299−310.

(36) Barone, V. M.; Cossi, M. *J. Phys. Chem. A* **1998**, *102*, 1995−2001.

(37) Barone, V. M.; Cossi, M.; Tomasi, J. *J. Chem. Phys.* **1997**, *107*, 3210−3221.

(38) Tannor, D. J.; Marten, B.; Murphy, R.; Friesner, R. A.; Sitkoff, D.; Nicholls, A.; Ringnalda, M.; Goddard, W. A., III; Honig, B. *J. Am. Chem. Soc.* **1994**, *116*, 11875−11882.

(39) Marten, B.; Kim, K.; Cortis, C.; Friesner, R. A.; Murphy, R. B.; Ringnalda, M.; Sitkoff, D.; Honig, B. *J. Phys. Chem.* **1996**, *100*, 11775−11788.

(40) Blomberg, M. R. A.; Siegbahn, P. E. M.; Babcock, G. T. *J. Am. Chem. Soc.* **1998**, *120*, 8812−8824.

(41) Siegbahn, P. E. M.; Blomberg, M. R. A. *Annu. Rev. Phys. Chem.* **1999**, *50*, 221−249.

(42) Siegbahn, P. E. M.; Blomberg, M. R. A. *Chem. Rev.* **2000**, *100*, 421−437.

(43) Blomberg, M. R. A.; Siegbahn, P. E. M. *J. Phys. Chem. B* **2001**, *105*, 9375−9386.

(44) Prabhakar, R.; Siegbahn, P. E. M. *J. Phys. Chem. B* **2001**, *105*, 4400−4408.

(45) Fontecave, M.; Eklund, H. *Structure* **1995**, *3*, 1127−1129.
(46) Wilmot, C. M.; Hajdu, J.; McPherson, M. J.; Knowles, P. F.; Phillips, S. E. V. *Science (Washington, D.C.)* **1999**, *286*, 1724−1728.
(47) Siegbahn, P. E. M. *J. Am. Chem. Soc.* **1998**, *120*, 8417−8429.
(48) Himo, F.; Siegbahn, P. E. M. *J. Phys. Chem. B* **2000**, *104*, 7502−7509.
(49) Himo, F.; Eriksson, L. A. *J. Am. Chem. Soc.* **1998**, *120*, 11449−11455.